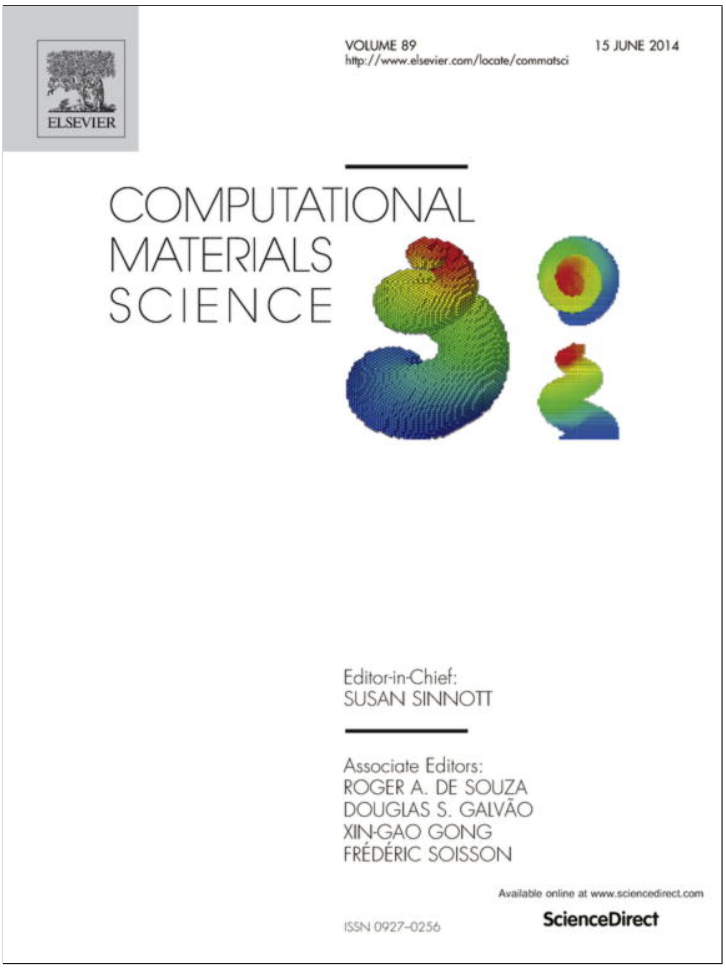

Computational Materials Science 89 (2014) 45–51

Contents lists available at ScienceDirect

Computational Materials Science

journal homepage: www.elsevier.com/locate/commatsci

Electronic structure and dispersion of optical function of tantalum nitride as a visible light photo-catalyst

A.H. Reshak *

New Technologies – Research Center, University of West Bohemia, Univerzitni 8, 306 14 Pilsen, Czech Republic
Center of Excellence Geopolymer and Green Technology, School of Material Engineering, University Malaysia Perlis, 01007 Kangar, Perlis, Malaysia

ARTICLE INFO

Article history:
Received 30 November 2013
Received in revised form 15 March 2014
Accepted 18 March 2014
Available online 13 April 2014

Keywords:
Photocatalyst
Visible light irradiation
DFT
Ta_3N_5

ABSTRACT

Tantalum nitride Ta_3N_5, as a visible light photocatalyst is studied using the state-of-the-art full potential linear augmented plane wave (FPLAPW) method in a scalar relativistic version. The calculated energy band gap values are vary between 1.1 eV (LDA), 1.2 eV (GGA), 1.5 eV (EVGGA) and 2.1 eV (mBJ). The band gap obtained using mBJ show excellent agreement with the experimental value 2.1 eV than the previous calculation. Thus mBJ potential is applied to investigate the ground state properties of tantalum nitride. The conduction band minimum is located at Y point of BZ, while the valence band maximum is located at the center of BZ indicates that the tantalum nitride is an indirect band gap semiconductor. The calculated electron charge density contours show that covalent bond exist between Ta and N atoms. The optical properties are discussed in details to seek deeper insight for the electronic structure. The calculated uniaxial anisotropy of Ta_3N_5, indicate a strong anisotropy of the optical dielectric functions. The absorption spectrum show that the absorption occurs in the visible region which makes Ta_3N_5 as an active photocatalyst under visible light irradiation. Ta_3N_5 crystal almost behaves as transparent in the higher wavelength light.

1. Introduction

The depletion of fossil fuels and environmental problems has greatly diverted the attention of researchers towards the clean, renewable and suitable alternative to fossil fuels. Hydrogen is considered to be the next generation energy carrier. Photocatalysis, the overall splitting of water is the potential method for production of hydrogen. Tantalum nitrides have attracted great deal of interest recently due to its potential technological application. It exhibits a remarkable richness with regard to the array of equilibrium and metastable phases that can form [1,2]. Among many applications of tantalum nitrides includes diffusion barrier in integrated circuit, wear-resistance layer, used as coating in cutting tools, thin film resisters [3]. TaN also gain its importance due to its growing interest regarding its potential as electronic materials especially as barrier layer in josephson junctions, consist of superconductor/normal-conductor/superconductor (SNS) interfaces which are of great interest in connection with high speed digital electronics [4]. Takata et al. found that TaON and Ta_3N_5 evolve O_2 or H_2 through band gap excitation in the presence of sacrificial electron donor or accepter respectively. These materials remain stable against photo-corrosion under the reaction conditions for H_2 and O_2 evolution [5]. Tantalum nitride (Ta_3N_5) is considered as the pigment material [6]. It has an orthorhombic crystal structure as determined by Brese and O'Keeffe using time of flight neutron diffraction [7]. The structure of Ta_3N_5 is composed of irregular octahedron of N atoms centered by Ta atoms [7,8]. The difficulty in the developing the successful photocatalysts is due to the lack of fundamental requirements such as band edge potentials suitable for the overall splitting of water, energy band gap (E_g) smaller than 3.0 eV and stability of the materials in the photocatalytic reaction [9–22]. The water splitting reaction on a semiconductor photocatalyst is performed in three steps (a) the photocatalyst absorbs photon energy greater than the band gap energy of the materials and generated photoexcited electron–hole pairs in the bulk. (b) The photoexcited carrier separate and move to the surface without recombination. (c) Absorbed species are reduced and oxidized by the photo-generated electrons and holes to produce H_2 and O_2 respectively. The electronic and structural properties of the photocatalyst play important role in the first two steps. High crystallinity of the structure has a great effect on the activity since the density of defects decreases with the increasing crystallinity. The last step occurs due to the presence of solid catalyst [23]. Terao [2] reported many phases of tantalum nitride which were prepared by nitriding

* Address: New Technologies – Research Center, University of West Bohemia, Univerzitni 8, 306 14 Pilsen, Czech Republic. Tel.: +420 777 729 583.
E-mail address: maalidph@yahoo.co.uk

http://dx.doi.org/10.1016/j.commatsci.2014.03.035
0927-0256/

evaporated Ta films in an atmosphere of ammonia and nitrogen. $TaN_{-0.5}$, Ta_2N, Ta_5N_6, Ta_4N_5 and Ta_3N_5 phases were obtained at the temperature range of 600–1100 °C [2]. From above we notice that there is dearth of information about the electronic structure and optical properties of tantalum nitride as a visible light photocatalyst. Therefore we thought it would be worthwhile to perform comprehensive theoretical calculations based on the self-consistent first principle calculations to obtain comprehensive information about the crystal structure, electronic band structure and optical properties of tantalum nitride, Ta_3N_5.

The main goal of the present work is to investigate the electronic band structure and the dispersion of optical properties of tantalum nitride, Ta_3N_5 as a visible light photocatalyst to solve the environmental problems and use it as clean and renewable alternative resources to fossil fuels.

2. Structural properties and computational details

The state-of-the-art full potential linear augmented plane wave (FPLAPW) method in a scalar relativistic version within the frame work of density functional theory (DFT) as implemented in the WIEN2k package [24] was employed. We have calculated the electronic band structure, total and partial density of states, the electronic charge density distribution and the dispersion of optical properties for tantalum nitride, Ta_3N_5. The exchange correlation potential were treated by four kind of approximations namely local density approximation (LDA) the Ceperley–Alder (CA) approach, generalized gradient approximation (GGA-PBE) the Perdew Becke Ernzerhof approach, Engel Vosko generalized gradient approximation (EVGGA) and the modified Becke–Johnson potential (mBJ). We treat the core states fully relativistically and the valence state scalar relativistically. The value of the angular momentum is taken to be $\ell = 10$ inside the muffin-tin spheres for both the wave-function and charge density in the self-consistent cycles. Basis set convergence was controlled by the cutoff parameter $R_{mt}K_{max} = 7$. Where R_{mt} represent smallest atomic sphere radius in the unit cell and K_{max} is the magnitude of the largest K vector. Calculations were performed using 168 K point mesh in the irreducible Brillouin zone (IBZ). The self-consistent convergence accuracy was set at 10^{-4} Ry. Since the value of the energy gap is very crucial for the photocatalysts, therefore we need to calculate the exact and accurate value of the energy band gap. Thus the mBJ considered to be one among the best approximations in obtaining very accurate results. The mBJ, a modified Becke–Johnson potential, allows the calculation of band gaps with accuracy similar to the very expensive GW calculations [25]. It is a local approximation to an atomic "exact-exchange" potential and a screening term. In 1991, Brese and O'Keeffe [7] reported that the tritantalum pentanitride (Ta_3N_5) has been prepared from the reaction of $TaCl_5$ with ammonia and refined structure was obtained by time of flight neutron diffraction data. They found that the crystal structure of Ta_3N_5 is orthorhombic with space group *Cmcm* (see Fig. 1). The atomic positions and lattice constants are given in Table 1.

3. Results and discussion

3.1. Band structure and density of states

Electronic band structure play vital role in studying the materials and show the value of energy gap E_g between the conduction

Table 1
Lattice parameter and atomic positions of Ta_3N_5 [7].

Lattice parameter (Å)		*a* 3.8862	*b* 10.2118	*c* 10.2624
Atom	Wyckoff sites	x	y	z
Ta1	4c	0	0.1971	0.25
Ta2	8f	0	0.13455	0.55906
N1	4c	0	0.76322	0.25
N2	8f	0	0.04701	0.11949
N3	8f	0	0.30862	0.073378

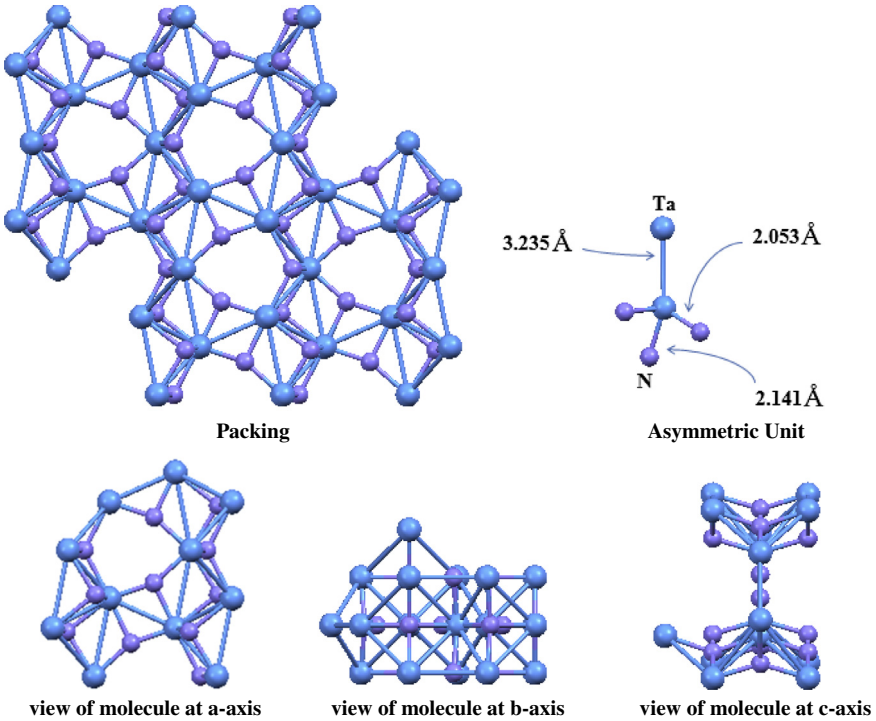

Fig. 1. Unit cell structure of Ta_3N_5.

and valence band. We apply four types of exchange and correlations namely; LDA, GGA, EVGGA and mBJ in order to get accurate band gap value for Ta_3N_5 in comparison to the experimental once. As we shift from one approximation to another we get better band gap's value till we reach close to the experimental value. The calculated electronic energy band structure using different schemes is displayed in Fig. 2(a–d). From Fig. 2, one can see that the conduction band minimum (CBM) is located at *Y* point of BZ, while the valence band maximum (VBM) is situated at the center of BZ, resulting in an indirect band gap. The energy band gap values are 1.1 eV (LDA), 1.2 eV (GGA), 1.5 eV (EVGGA) and 2.1 eV (mBJ). The underestimation of band gap by DFT is common which exist due to the limitation of predicting conduction band properties [26]. Our calculated energy gap value using mBJ is 2.1 eV shows excellent agreement with the experimental value 2.1 eV [27], and much better than previous theoretical values 1.1 eV obtained by using VASP code and 1.2 eV obtained by using WIEN97 [28]. Useful information can be gain from total density of states (TDOS) and partial density of states (PDOS) such as hybridization of states, bonding nature and contribution of orbitals to the electronic band structure. Fig. 3 illustrates the TDOS and PDOS of Ta, and N in Ta_3N_5. The PDOS express that valence band maximum is mostly dominated by N_1-p, N_2-p and Ta-d states in the energy range −6.0 and 0.0 eV. While the bottom of the conduction band is composed of Ta-d and N_1-p orbitals between 2.0 eV and 11.0 eV. In the lower energy between −16.0 eV and −13.0 eV, N_1-s orbital and N_2-s orbitals mainly contribute and a small participation from Ta-p state can also be observe. The contribution of Ta-s and Ta-f orbitals to the conduction band and valence band is very small. Strong hybridization means potential covalent bonding and less ionic character. Covalent bond is formed between N and Ta atoms as can be seen from PDOS when N_2-p and Ta-d states hybridized in the energy range between −5.0 eV and −4.0 eV. N_1-s and N_2-p orbitals show strong hybridization in the energy range between 7.0 eV and 8.0 eV.

3.2. Electronic charge density

The electronic charge density distribution has been calculated in (100) crystallographic plane by using mBJ approach (see Fig. 4). One can easily predict the bonding nature and charge transfer between atoms from the electronic charge density distribution. As greater electronegativity difference (ΔEN) assure ionic bonding, and less ΔEN show the presence of covalent bond between atoms. The electronegativity values of Ta and N are as follow 1.5 and 3.04 respectively. The ΔEN between Ta and N is 1.54 which shows covalent nature of bond between these atoms. From the electronegativity difference we can find out the percent of ionic character. The percent ionicity from the ΔEN between Ta and N is 32.94% resulting in greater percentage of covalency, 67.06%. The effect of most electronegative element to attract electron towards itself can easily be seen from the charge density plot in (100) crystallographic plane. From the thermo-scale, the colors represent different charge concentration areas. Blue color is the

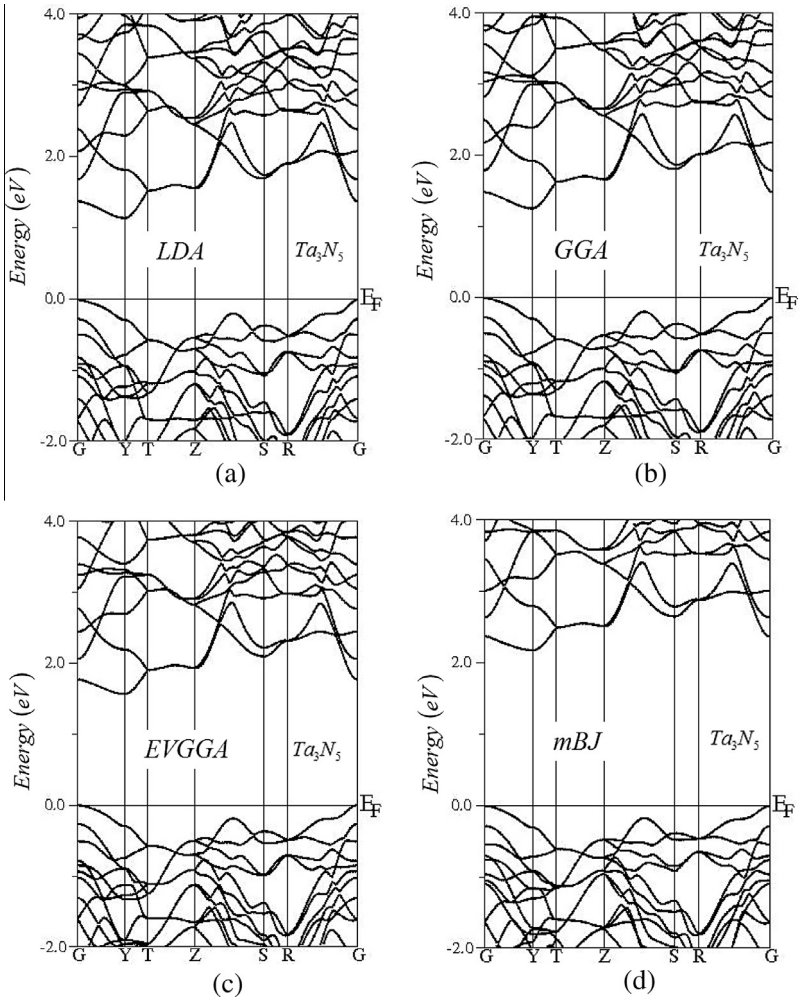

Fig. 2. Calculated band structure of Ta_3N_5 compound.

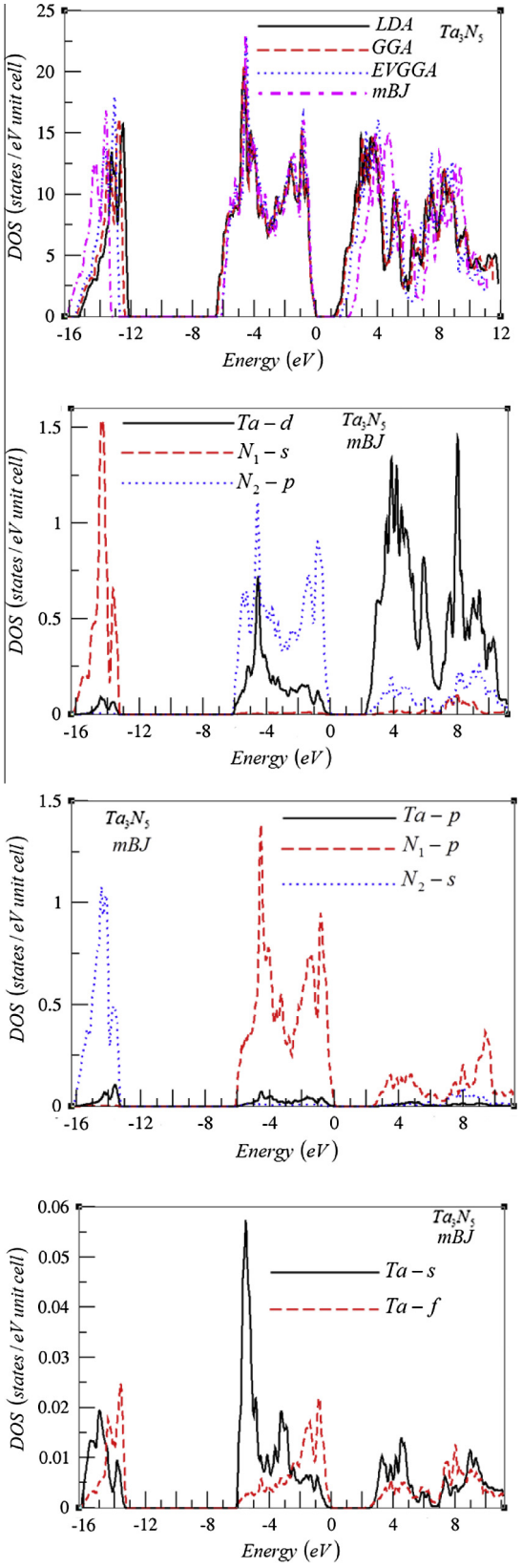

Fig. 3. Calculated Total density of states (states/eV unit cell) and PDOS of Ta_3N_5.

maximum charge representative. This means maximum charge gathered around nitrogen as nitrogen is high electronegative element. Electron charge density contours show that covalent bond exist between Ta and N atoms.

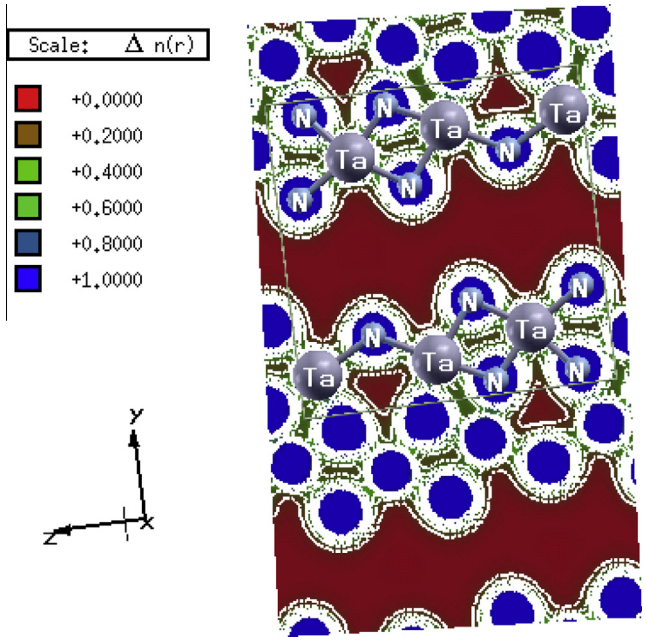

Fig. 4. Electronic charge density of Ta_3N_5.

3.3. Optical properties

The development of photocatalysts that work under visible light to efficiently utilize the solar energy is very crucial and promising for clean and sustainable energy. The difficulty in the developing the successful photocatalysts is due to the lack of fundamental requirements such as band edge potentials suitable for the overall splitting of water, band gap energy (E_g) smaller than 3.0 eV and stability of the materials in the photocatalytic reaction [9–22]. Therefore we need to search for novel materials which absorb photons of wavelength between 400 and 700 nm and possess an optical band gap vary between 1.77 and 3.1 eV. Thus we need optically active materials in the visible region, in the following paragraphs we will shed more light on the optical properties. The optical properties can provide detailed information about the electronic structure of the materials. The optical properties of solids are a major topic, both in basic research as well as for industrial applications. While for the former the origin and nature of different excitation processes is of fundamental interest, the latter can make use of them in developing the photocatalysts. We should emphasize that the nitride crystals possess very specific features which consists in the delocalized states of nitrogen [29] that influence the optical properties due to changes of the corresponding transition moments.

Since Ta_3N_5 crystallizes in *Cmcm* orthorhombic space group. This space groups allows only three non-zero tensor components for the second-order dielectric tensor corresponding to the electric field $\vec{E}$ being directed along **a**, **b**, and **c**-crystallographic axes. We will assume that these are the *x*, *y*, *z* components. These are the principal diagonal tensor components, $\varepsilon^{xx}(\omega)$, $\varepsilon^{yy}(\omega)$ and $\varepsilon^{zz}(\omega)$ which completely define the dispersion of linear optical susceptibilities.

Fig. 5(a) and (b) shows the calculated $\varepsilon_2^{average}(\omega)$ of $\varepsilon_2^{xx}(\omega)$, $\varepsilon_2^{yy}(\omega)$ and $\varepsilon_2^{zz}(\omega)$ components and $\varepsilon_1^{average}(\omega)$ of $\varepsilon_1^{xx}(\omega)$, $\varepsilon_1^{yy}(\omega)$ and $\varepsilon_1^{zz}(\omega)$ components using LDA, GGA, EVGGA and mBJ. The real part is determined from the imaginary part by using the Kramer-Kronig transformation. Both of $\varepsilon_2^{average}(\omega)$ and $\varepsilon_1^{average}(\omega)$ spectra confirm that the mBJ approach bring the energy gap close to the experimental once. This can be clearly observe from the calculated value of $\varepsilon_1^{average}(0)$. These values as listed in Table 2, show that a smaller

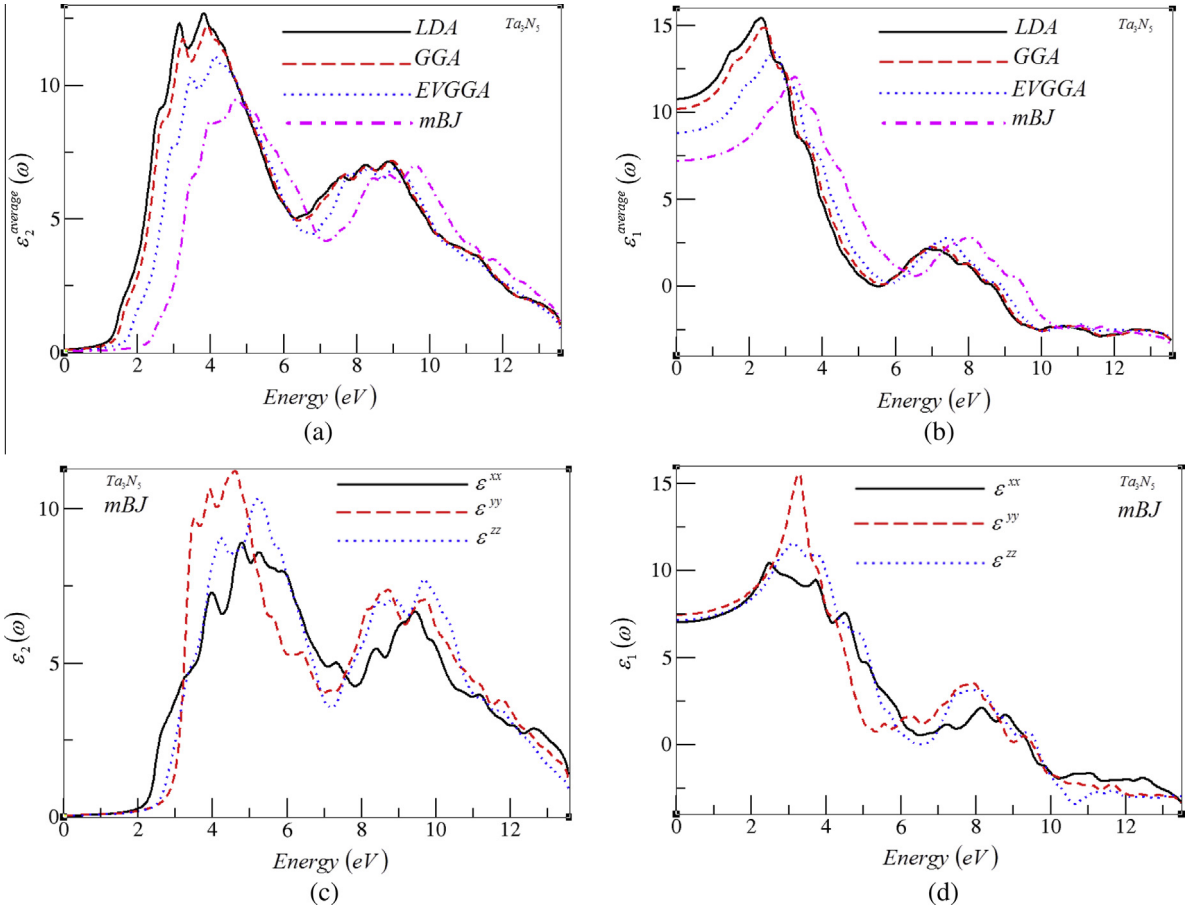

Fig. 5. Calculated $\varepsilon_2^{average}(\omega)$, $\varepsilon_2(\omega)$,$\varepsilon_1^{average}(\omega)$ and $\varepsilon_1(\omega)$ for Ta_3N_5.

energy gap yields a larger $\varepsilon_1(0)$ value. This could be explained on the basis of the Penn model [30]. Penn proposed a relation between $\varepsilon(0)$ and E_g, $\varepsilon(0) \approx 1 + (\hbar\omega_P/E_g)^2$. E_g is some kind of averaged energy gap which could be related to the real energy gap. It is clear that $\varepsilon(0)$ is inversely proportional with E_g. Hence a smaller E_g yields a larger $\varepsilon(0)$. Following what we have observed from Fig. 5(a) and (b), that mBJ produce better band gap and hence better optical transitions. Thus we decided to show only the results obtained by mBJ. Fig. 5c show the calculated $\varepsilon_2(\omega)$ using mBJ approach, the spectral structures of the three components show two main peaks, one located at lower energies around 4.0 eV for $\varepsilon_2^{xx}(\omega)$ and $\varepsilon_2^{yy}(\omega)$ and around 5.0 eV for $\varepsilon_2^{zz}(\omega)$. The second peak is located at higher energies around 9.0 eV for both of $\varepsilon_2^{xx}(\omega)$ and $\varepsilon_2^{yy}(\omega)$ and at 10.0 for $\varepsilon_2^{zz}(\omega)$.. Transition between Ta-d and N_2-p states of anions mainly contribute to the peaks occurs in imaginary part $\varepsilon_2(\omega)$ at around 4.0 eV and 10.0 eV. The principal complex tensor components show considerable anisotropy. The real part $\varepsilon_1(\omega)$ is calculated using mBJ, again it confirm the considerable anisotropy among $\varepsilon_1^{xx}(\omega)$, $\varepsilon_1^{yy}(\omega)$ and $\varepsilon_1^{zz}(\omega)$.. The calculated values of $\varepsilon_1^{xx}(0)$, $\varepsilon_1^{yy}(0)$ and $\varepsilon_1^{zz}(0)$ using LDA, GGA, EVGGA and mBJ are listed in Table 2. The uniaxial anisotropy $\delta\varepsilon = (\varepsilon_0^{ll} - \varepsilon_0^{\perp})/\varepsilon_0^{tot}$ which is indicating the strong anisotropy of the dielectric function is calculated and listed in Table 2.

Table 2
Calculated $\varepsilon_1^{average}(0)$, $\varepsilon_1^{xx}(0)$, $\varepsilon_1^{yy}(0)$, $\varepsilon_1^{zz}(0)$ $n^{xx}(0)$, $n^{yy}(0)$, and $n^{zz}(0)$.

$\varepsilon_1^{average}(0)$	LDA 10.80	GGA 10.30	EVGGA 8.80	mBJ 7.20
$\varepsilon_1^{xx}(0)$	10.90	10.30	8.80	7.10
$\varepsilon_1^{yy}(0)$	11.01	10.40	9.10	7.40
$\varepsilon_1^{zz}(0)$	10.44	9.90	8.60	7.30
$\delta\varepsilon = (\varepsilon_0^{ll} - \varepsilon_0^{\perp})/\varepsilon_0^{tot}$	−0.047	−0.043	−0.039	0.007
$n^{xx}(0)$	3.30	3.21	2.97	2.65
$n^{yy}(0)$	3.32	3.23	3.01	2.73
$n^{zz}(0)$	3.23	3.15	2.93	2.68
$n^{average}(0)$	3.28	3.19	2.97	2.68
$\Delta n(\omega)$	−0.08	−0.07	−0.06	−0.01

The reflectivity $R(\omega)$ is plotted in Fig. 6(a) as a function of wavelength in which $R^{yy}(\omega)$ is the dominant component between 250 nm and 450 nm of the spectrum. Maximum reflectivity value for all components occur at about 90 nm also there observed two minor peaks at around 230 nm for $R^{zz}(\omega)$ and at 250 nm for $R^{yy}(\omega)$. Above 450 nm the spectrum of all components remains constant. The absorption coefficient $I(\omega)$ measure the penetration of light through materials before it gets absorbed. We have calculated the absorption coefficient in term of wavelength (nm) (see Fig. 6(b)), one can see that the $I(\omega)$ rapidly increases above 90 nm and reaches its maximum value at around 140 nm. From the absorption spectrum we can see that absorption occurs in the visible region which makes Ta_3N_5 as an active photocatalyst under visible light irradiation. Ta_3N_5 crystal almost behaves as transparent in the higher wavelength light. The absorption band extends from 90 nm to 450 nm.

The refractive index $n(\omega)$, extinction coefficient $k(\omega)$ and energy loss function $L(\omega)$ are calculated and illustrated in Fig. 7(a–c). The complex refractive index $(\tilde{n}(\omega) = n(\omega) + ik(\omega))$ describes the refraction as well as the absorption of the compounds. It

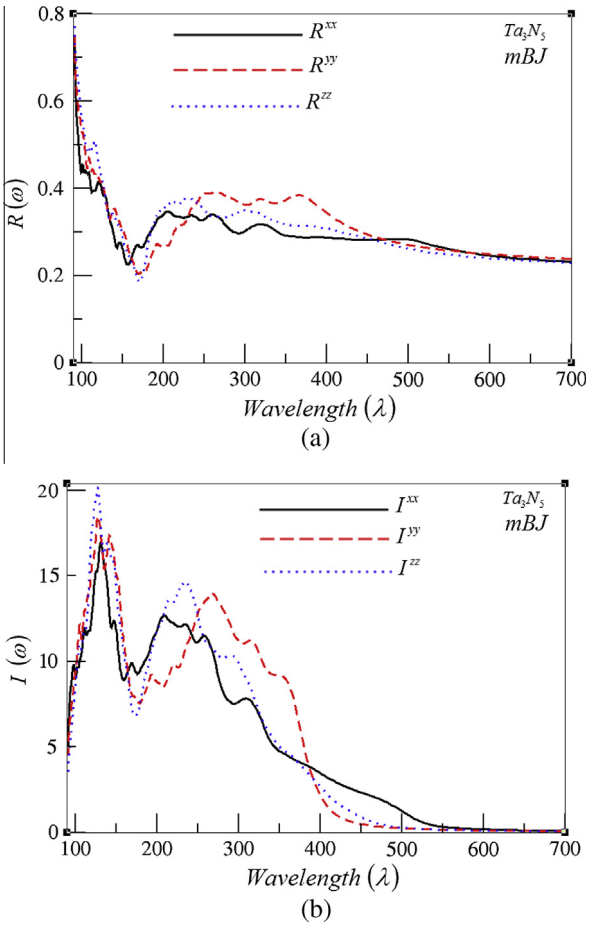

Fig. 6. Reflectivity and Absorption coefficient. (a) $R(\omega)$ and (b) $I(\omega)$.

consists of two parts, first the real part, $n(\omega)$, is just the ordinary refractive index while the second part, $k(\omega)$, is the extinction coefficient which describe the loss of photon energy as it propagate through the optical medium. As Ta_3N_5 compound has orthorhombic symmetry, therefore three tenser components are required to completely describe the optical properties. The x, y z components of refractive index and extinction coefficient as a function of energy are plotted in Fig. 7(a) and (b). The refractive indices at static limit $n^{xx}(0)$ and $n^{yy}(0)$ and $n^{zz}(0)$ are calculated and listed in Table 2. The calculated average value of refractive index at static limit $n(0)$ of Ta_3N_5 is about 2.68. From the values of the refractive indices at static limit one can calculate the birefringence $\Delta n(0)$ as listed in Table 2. The refractive indices increase beyond the zero frequency limits and reached to their maximum values. Beyond the maximum value they start to decrease and with few oscillations they go beyond unity. In this region ($n < 1$) the phase velocity of the photons increases to universal constant (C). However the group velocity always less than the C, therefore the relativity relations not effected [31]. Extinction coefficient $k(\omega)$ shows the absorption of compounds. It is seen from Fig. 7b) that the absorption edges are 2.2 eV for $k^{xx}(\omega)$, 2.7 eV for $k^{yy}(\omega)$, and 2.6 eV for $k^{zz}(\omega)$. Beyond the critical points, the absorption increases and become maximum at some particular energy, and then it decreases with small oscillations. The absorption peaks occurs at around 5.0 eV and 10.0 eV. Energy loss by the electron as it passes through the crystal is defined by optical parameter called energy loss function $L(\omega)$. Following Fig. 7(c), the peaks in the $L(\omega)$ indicates trailing edges in the reflectivity structure such as the reduction of $R(\omega)$ at around 104 nm till 160 nm wavelength corresponds to the peaks at about 12.5 eV and 7.0 eV in $L(\omega)$.

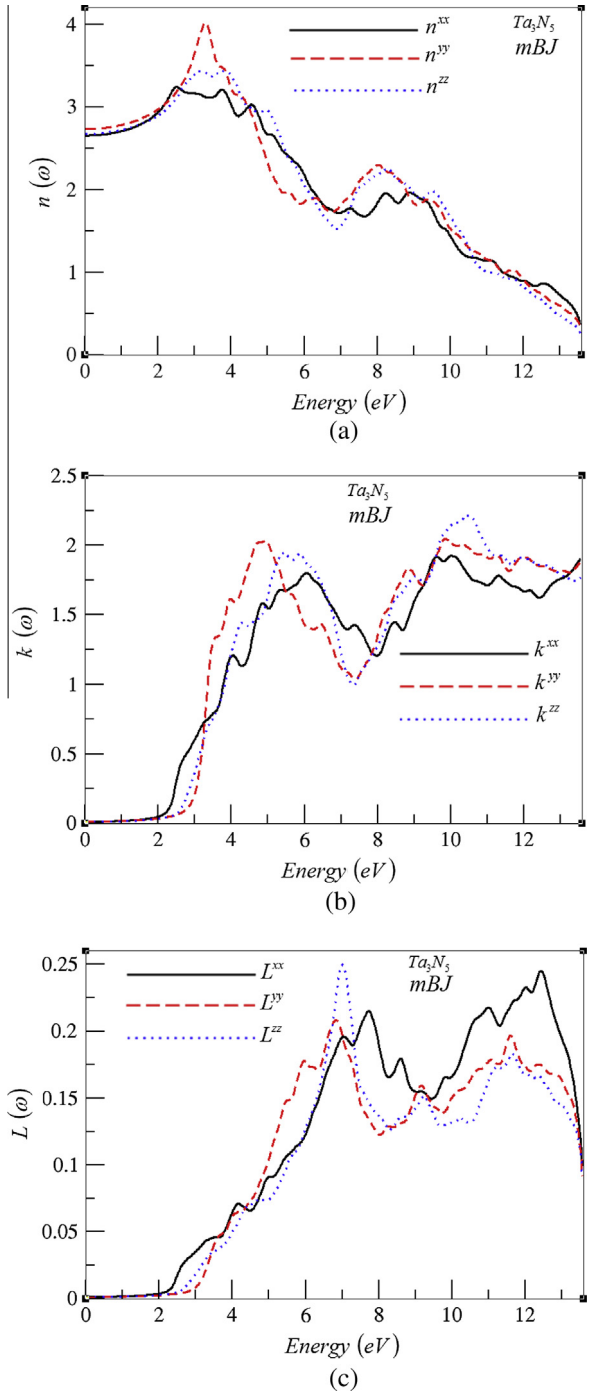

Fig. 7. Refractive index $n(\omega)$, extinction coefficient $k(\omega)$ and energy loss function $L(\omega)$.

4. Conclusions

First principles calculations were performed for Ta_3N_5 compound using FP-LAPW within DFT. We have calculated electronic band structure, total and partial density of states, electronic charge density distribution and the dispersion of the optical properties for Ta_3N_5 as a visible light photocatalyst. Due to its specialty, mBJ presents better band gap value close to experimental result as compared to other approximations namely LDA, GGA and EVGGA. The successful value of band gap using mBJ for Ta_3N_5 is 2.1 eV which is agree well with the experimental result 2.1 eV and much better then the previous calculations. The band gap is indirect as the CBM is situated at point Y and VBM occur at the center of

the Brilliouin zone. From the partial DOS we observed that valence band maximum is mostly dominated by N-p, and Ta-d states in the energy range between −6.0 and 0.0 eV. Hybridization of the states shows that covalent bond exist between Ta and N. electronic charge density contour plots represents covalent nature of chemical bonding. We found the refractive index for Ta_3N_5 and it bear 2.68 value in this calculation. The calculated absorption spectrum confirms that Ta_3N_5 compound is an active photocatalyst under visible light irradiation. The energy loss function and extinction coefficient is also calculated and discussed in details. The peaks in the energy loss function represent reduction in the trailing edges of reflectivity spectrum. The dispersion of the optical functions show that there exists a strong anisotropy between the three polarization directions which confirmed by the calculated value of the uniaxial anisotropy and the birefringence.

Acknowledgements

The result was developed within the CENTEM Project, Reg. No. CZ.1.05/2.1.00/03.0088, co-funded by the ERDF as part of the Ministry of Education, Youth and Sports OP RDI programme.

References

[1] C.-S. Shin, Y.-W. Kim, D. Gall, J.E. Greene, I. Petrov, Thin Solid Films 172–182 (2002) 402.
[2] N. Terao, Jpn. J. Appl. Phys. 10 (1971) 248–259.
[3] M.H. Tsai, S.C. Sun, C.P. Lee, H.T. Chiu, C.E. Tsai, S.H. Chuang, S.C. Wu, Thin Solid Films 270 (1995) 531–536.
[4] K. Likharev, Phys. World 10 (5) (1997) 39–43.
[5] T. Takata, G. Hitoki, J.N. Kondo, M. Hara, H. Kobayashi, K. Domen, Res. Chem. Intermed. 33 (1–2) (2007) 13–25.
[6] M. Jansen, H.P. Letschert, E.P. Patent 592867 (1993) A1.
[7] N.E. Brese, M. O'Keeffe, Acta Crystallogr. C47 (1991) 2291–2294.
[8] J. Strähle, Z. Anorg. Allg. Chem. 402 (1974) 47–57.
[9] J. Yoshimura, Y. Ebina, J. Kondo, K. Domen, A. Tanaka, J. Phys. Chem. 97 (1993) 1970–1973.
[10] A. Kudo, I. Mikami, Chem. Lett. 27 (1998) 1027–1028.
[11] A. Kudo, K. Ueda, H. Kato, I. Mikami, Catal. Lett. 53 (1998) 229–230.
[12] A. Kudo, K. Omori, H. Kato, J. Am. Chem. Soc. 121 (1999) 11459–11467.
[13] K. Sayama, K. Mukasa, R. Abe, Y. Abe, H. Arakawa, Chem. Commun. (2001) 2416–2417.
[14] H. Kato, A. Kudo, J. Phys. Chem. B 106 (2002) 5029–5034.
[15] H. Kato, H. Kobayashi, A. Kudo, J. Phys. Chem. B 106 (2002) 12441–12447.
[16] Y. Hosogi, K. Tanabe, H. Kato, H. Kobayashi, A. Kudo, Chem. Lett. 33 (2004) 28–29.
[17] R. Konta, T. Ishii, H. Kato, A. Kudo, J. Phys. Chem. B 108 (2004) 8992.
[18] H.G. Kim, D.W. Hwang, J.S. Lee, J. Am. Chem. Soc. 126 (2004) 8912–8913.
[19] H. Kato, M. Hori, R. Konta, Y. Shimodaira, A. Kudo, Chem. Lett. 33 (2004) 1348–1349.
[20] D.W. Hwang, H.G. Kim, J.S. Lee, J. Kim, W. Li, S.H.J. Oh, Phys. Chem. B 109 (2005) 2093–2102.
[21] H.G. Kim, P.H. Borse, W. Choi, J.S. Lee, Angew. Chem. Int. Ed. 44 (2005) 4585–4589.
[22] R. Abe, K. Sayama, H. Sugihara, J. Phys. Chem. B 109 (2005) 16052–16061.
[23] Kazuhiko Maeda, Kazunari Domen, J. Phys. Chem. C 111 (2007) 7851–7861.
[24] P. Blaha, K. Schwarz, G.K.H. Madsen, D. Kvanicka, J. Luitz, WIEN2K, Techn. Universitat, Wien, Austria, 2001. ISBN: 3-9501031-1-1-2.
[25] Fabien Tran, Peter Blaha, Phys. Rev. Lett. 102 (2009) 226401–226404.
[26] R.M. Martin, Electronic Structure: Basic Theory and Practical Methods, Cambridge University Press, Cambridge, England, 2004.
[27] N. Diot, Ph. D Dissertation, University of Rennes, 1 (1999) 127.
[28] C. M. Fang, E. Orhan, G. A. de Wijs, H. T. Hintzen, R. A. de Groot, R. Marchand, J.-Y. Saillard, G. de. J. Mater. Chem. 11 (2001) 1248–1252.
[29] I.V. Kityk, Comput. Mater. Sci. 27 (2003) 342.
[30] D.R. Penn, Phys. Rev. B 128 (1962) 2093–2097.
[31] M. Fox, Optical Properties of Solids, Oxford University Press, 2001.